ARCHIVES
of
FOUNDRY ENGINEERING

ISSN (2299-2944)

10.24425/afe.2025.155354

Published quarterly as the organ of the Foundry Commission of the Polish Academy of Sciences

Research on Casting Process of Electrolytic Aluminum Anode Phosphorus Cast Iron and Carbon Block based on ProCAST

Kun Zhang [a], Rong Li [b, *]

[a] Shenyang Aluminum & Magnesium Engineering & Research Institute Co., Ltd, China
[b] School of Mechanical & Electrical Engineering, Guizhou Normal University, China
* Corresponding author: E-mail address: lirong9242001@163.com

Received 24.12.2024; accepted in revised form 26.03.2025; available online 23.07.2025

Abstract

In order to obtain a better connection state between the carbon block and steel claw of aluminum guide rod in the electrolytic aluminum anode assembly, the casting simulation software (ProCAST) was used to simulate the casting process of phosphorus cast iron at different groove angles and the connection interface was actually detected. The results show that during the angle of phosphorus cast iron is 15 degrees, the filling speed, temperature distribution and the solid phase ratio are relatively uniform. Also, sequential solidification can be basically realized, which can lead to obtain the low porosity casting. The interface grain orientation between the phosphorus cast iron and the steel claw would be more dense, and the interface grain between the cast iron and the carbon block is more sparse. The simulation calculations are consistent with the actual EBSD test results. This process results in a good casting junction interface and retains the required brittleness (easy to press off and recycle assembly).

Keywords: Casting simulation, Groove angle, Phosphorus cast iron, Grain orientation, EBSD

1. Introduction

Cast iron with phosphorus element (called phosphorus cast iron) contains a certain amount of phosphorus in the iron. It is mainly used in the anode assembly process in the electrolytic aluminium industry. During this process, anode carbon blocks are joined to conductor rods. The connection is made by pouring molten phosphorus cast iron into the gap between the steel claws and the carbon bowls, which, after cooling, integrates the conductor rods with the carbon blocks into a single unit ready for use in the electrolytic process.

There is a wealth of research on the application of anodes in the electrolytic aluminium industry [1-4], with many scholars also conducting studies on the phosphorus iron casting process. Li Tuofu et al [5] used the ANSYS finite element software to construct a three-dimensional thermal-electrical-stress coupling model and found that when the diameter of the steel claw remains unchanged, an increase in the thickness of phosphorus iron does not significantly affect the temperature field and stress distribution of the anode, but it significantly reduces the anode voltage drop. When the thickness of the phosphorus iron is kept constant and the diameter of the steel claw is increased, the maximum temperatures of the anode steel claw, carbon block and phosphorus iron, as well as the anode voltage, all decrease. Zhang Yanhua et al. [6] used ANSYS software to simulate different preheating temperatures of anode carbon blocks in aluminium electrolysis cells, analysed the influence of different preheating temperatures on the stress changes in the anode assembly, and optimised the anode cracking phenomenon and the phosphorus iron casting process. Huang

Yongbo et al [7] discussed the effects of the elements C, Si and P in phosphorus iron on its thermal expansion coefficient and resistivity. They found that when the carbon content is about 4.3%, increasing the content of these three elements in phosphorus iron can reduce its thermal expansion coefficient, and reducing the content of Si and P in phosphorus iron can reduce its resistivity.
Although many studies have been carried out on phosphor cast iron using finite element software, few studies have been carried out using specialised software such as ProCAST for both material property analysis and grain analysis. Therefore, this study employed the finite element software PROCAST to investigate the influence of the mould groove on the formation of phosphorus cast iron models during casting. In addition, the CAFE module is used to observe the microstructure of the formed phosphorus cast iron and compare it with EBSD images to understand the formation of grain boundaries on its surface.

2. Materials and Methods

2.1. Physical model

This project is concerned with the study of phosphorus cast iron, which is employed in the electrolytic aluminium industry for the purpose of connecting anode steel claws with carbon blocks. This material is renowned for its exceptional electrical conductivity and bonding strength, which ensure a uniform distribution of current across the various claws of the anode and thereby prevent anode detachment. It is of the utmost importance to meticulously oversee the pouring process during anode assembly in order to maintain the quality of the anode assembly and enhance the current efficiency of the electrolytic cell. Fig.1 depicts the physical model, which encompasses the anode carbon block, phosphorus cast iron, steel claw and conductor rod. The carbon block features a regular rectangular structure, adorned with four carbon bowls on its surface. The anode exhibits central symmetry about its central axis, with a uniform casting method applied to all four carbon bowls. Consequently, one carbon bowl is analyzed as a representative example. The detailed structural dimensions of the anode model are documented in Table 1.

The pouring analysis was conducted using the Procast software platform. Once the optimal angle for the carbon bowl's circumferential groove had been determined through pouring simulation, the CAFE module was employed to model the casting organisation's progression. Subsequently, the simulation was compared with the actual casting organisation observed post-inspection.

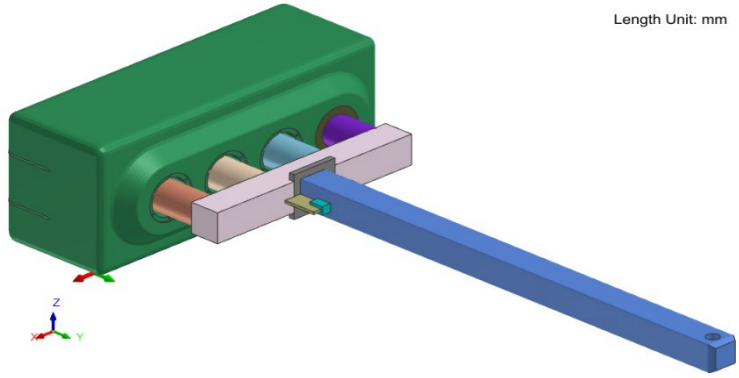

Fig.1. Physical model: 1-Anode carbon block, 2-Phosphorus cast iron, 3-Steel claw, 4- Aluminum guide rod

Table 1.
Structural Dimensions

Content	Anode carbon block	Diameter of steel claw	Diameter of carbon bowl	Length of guide bar	Guide bar cross section	Depth of carbon bowl
Size (mm)	710×750×1770	180	215	2615	160×165	130

2.2. Material Properties

In this physical model, the carbon block is predominantly composed of carbon. The anode clamp bar is fabricated from Q355B steel, while the anode rod is manufactured from aluminum. The sputtering material utilized for the phosphorus cast iron is phosphorus iron, with its primary chemical constituents detailed in Table 2.

Table 2.
Chemical composition of phosphorus cast iron

Name of element	C	S	Si	Mn	P	Fe
quantity (%)	3.23	0.11	2.42	0.71	0.52	Based

2.3. Design of Casting Programs

The objective of this investigation was to ascertain the influence of varying circumferential groove angles on the molding process of phosphorus cast iron pouring. This was done in order to guarantee the even and stable flow of molten iron into carbon blocks and to prevent casting defects like blowholes and slag inclusions. In order to achieve this, molds featuring diverse circumferential groove angles were fabricated while maintaining uniformity in other dimensional and shape aspects. Subsequently, software was employed to conduct a meticulous comparison of the casting outcomes across different angles, ensuring that all other parameters remained constant to preclude errors arising from parameter fluctuations. In accordance with the aforementioned stipulations, a series of comparative experiments was designed and is detailed in Table 3. Due to processing limitations, the angle intervals were defined as 5-degree increments, resulting in a total of six controlled experiments, beginning with 0 degrees, which represents vertical descent. Among them, combined with the actual casting test, the casting time set in the software is 6s, the casting temperature is about 1300°C, the mould material used is charcoal and steel, and the casting technology uses the cavity formed by the natural cooperation between the charcoal block and the steel claw for casting to ultimately achieve the purpose of casting moulding.

Table 3.
Angles of different casting mold solutions and schematic diagram

Casting mold angle	Schematic diagram
0°	
5°	
10°	
15°	
20°	
25°	

3. Simulation Results and Discussion

Prior to conducting the simulation calculation, it is of the utmost importance to establish the following boundary conditions for the pouring process. In accordance with the specifications outlined in the casting manual, the heat transfer coefficient between the steel claw and the phosphorus cast iron has been established at 3000 W/(m²·K), while the coefficient between the phosphorus cast iron, steel claw, and carbon block has been set at 1000 W/(m²·K). The simulation calculation will conclude upon the complete solidification of the phosphorus cast iron under natural air cooling conditions. The simulation is conducted using Procast2021 software.

3.1. Simulation Calculation Process

The primary steps of this casting simulation process are as follows: Firstly, the IGS file of the external product model generated by 3D software is imported into the ProCAST simulation software. Secondly, a CAD inspection and correction is conducted on the imported product model. Thirdly, the surface/volume mesh is divided and repaired. Fourthly, the software parameters are set according to the pouring method. Finally, the product pouring process is simulated. Fig.2 illustrates the mesh division of the phosphorus cast iron and anode carbon block assembly. As shown in Fig. 2. from the body mesh shown, from it can be seen that the thin-walled position mesh is multilayered, which can guarantee the accuracy of the calculation.

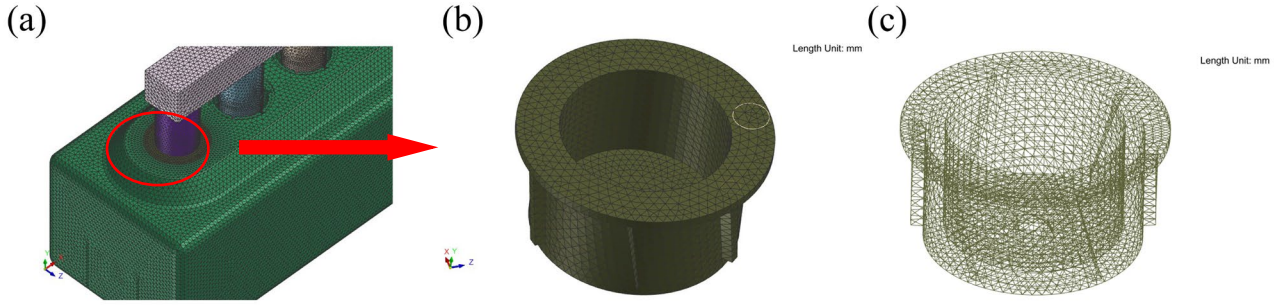

Fig. 2. Mesh division of the product model: (a) Anode carbon block assembly grid, (b) Phosphorus cast iron grid, (c) Body mesh

3.2. The Influence of Varying Size-To-Bore Angle Ratios on the Filling Procedure

This study examines the impact of varying carbon block circumferential groove angles on flow field dynamics and product quality[8, 9]. The soundness of the mold used to cast phosphorus cast iron is of great consequence with respect to the quality of the resulting product, as it often gives rise to a variety of casting imperfections. The study conducted a comprehensive examination of the melt's flow and temperature dynamics during and following the filling process, with the objective of identifying the optimal filling strategy.

3.2.1. Flow field state

The flow field of phosphorus cast iron castings, as derived from various molds and depicted in Fig.3. Reveals a casting filling process marked by its brevity, rapidity and smoothness; devoid of notable air entrapment or turbulent flow and a relatively smooth rate of rise.

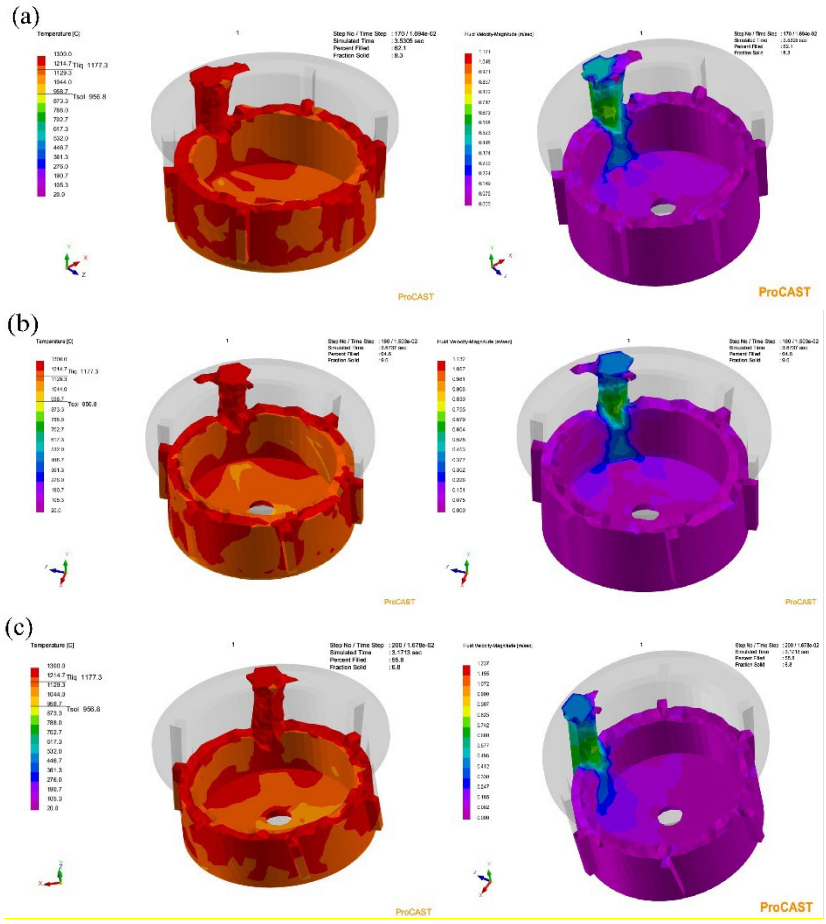

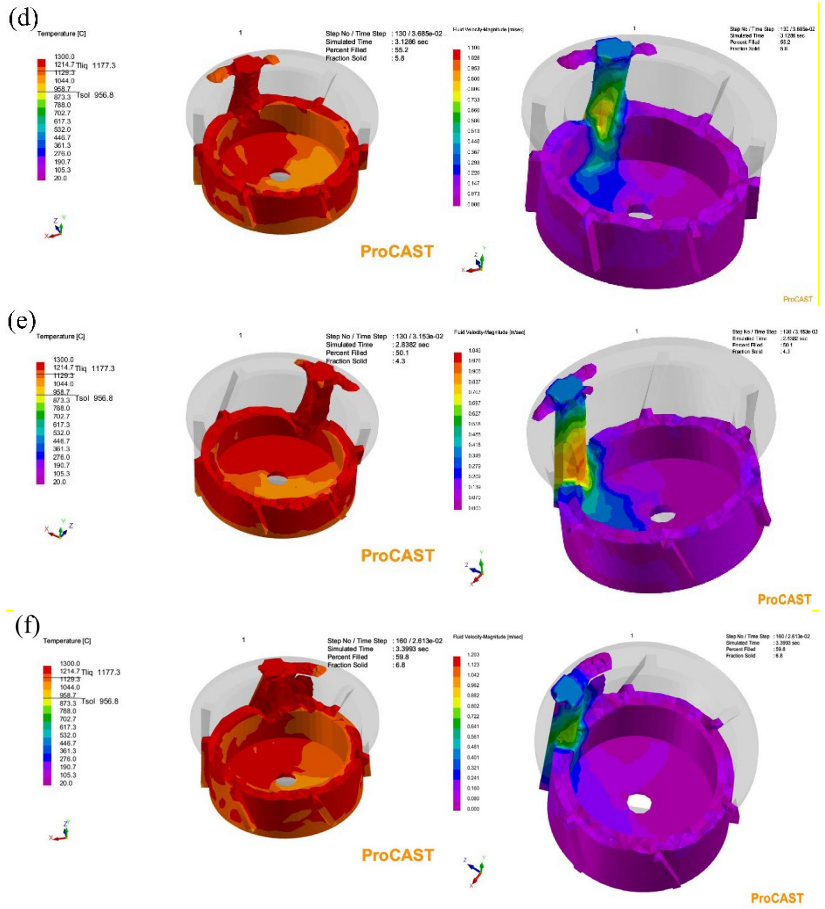

Fig. 3. Filling process of different mold schemes: (a) 0°, (b) 5°, (c) 10°, (d) 15°, (e) 20°, (f) 25°

As illustrated in the diagram, the liquid level within the cavity rises in a gradual and relatively unhurried manner. This gradual ascent enables the more straightforward expulsion of air and slag that may be entrapped within the cavity. In the event that the dimensions of the pouring inlet and the speed of the pouring process remain identical, the scenario in which the angle is 5 degrees entails the injection of liquid from the circumferential groove during the pouring process. As illustrated in Fig.3(c) to Fig.3(e), the velocity of the liquid column remains relatively uniform and its dimensions are also consistent in these three instances. It is evident that a reduction in the angle of the circumferential groove results in a more uniform liquid injection; which in turn leads to the production of phosphorus cast iron of superior quality.

The properties of molten metal fluid can be derived from the temperature range of alloy phase transitions. Furthermore, the casting filling process hinges on both the fluidity of the metal within the system and the geometry of the casting cavity. Consequently, uncontrolled fluid flow can induce turbulence, as illustrated in Fig.3(b). Such turbulence can result in the entrapment of air and slag within the casting cavity during the fluid filling process, which in turn can give rise to substantial oxide defects[10]. By a detailed examination of the flow of molten metal within the flow field, the behaviour of molten metal in the phosphorus cast iron cavity during the casting process can be fully elucidated. The speed and time required for the casting to be filled are affected by the circumferential groove angle of the mold, depending on the conditions of the mold. The manner in which the cavity is filled can affect the cooling rate of the casting, and may even alter the sequence of solidification of the casting.

3.2.2. Temperature field status

The temperature distribution in castings resulting from various mold configurations post-filling is depicted in Fig.4. The simulation outcomes indicated that upon completion of the casting process, the overall temperature of the castings remained above the metal's solidus line, approximating the liquidus line.

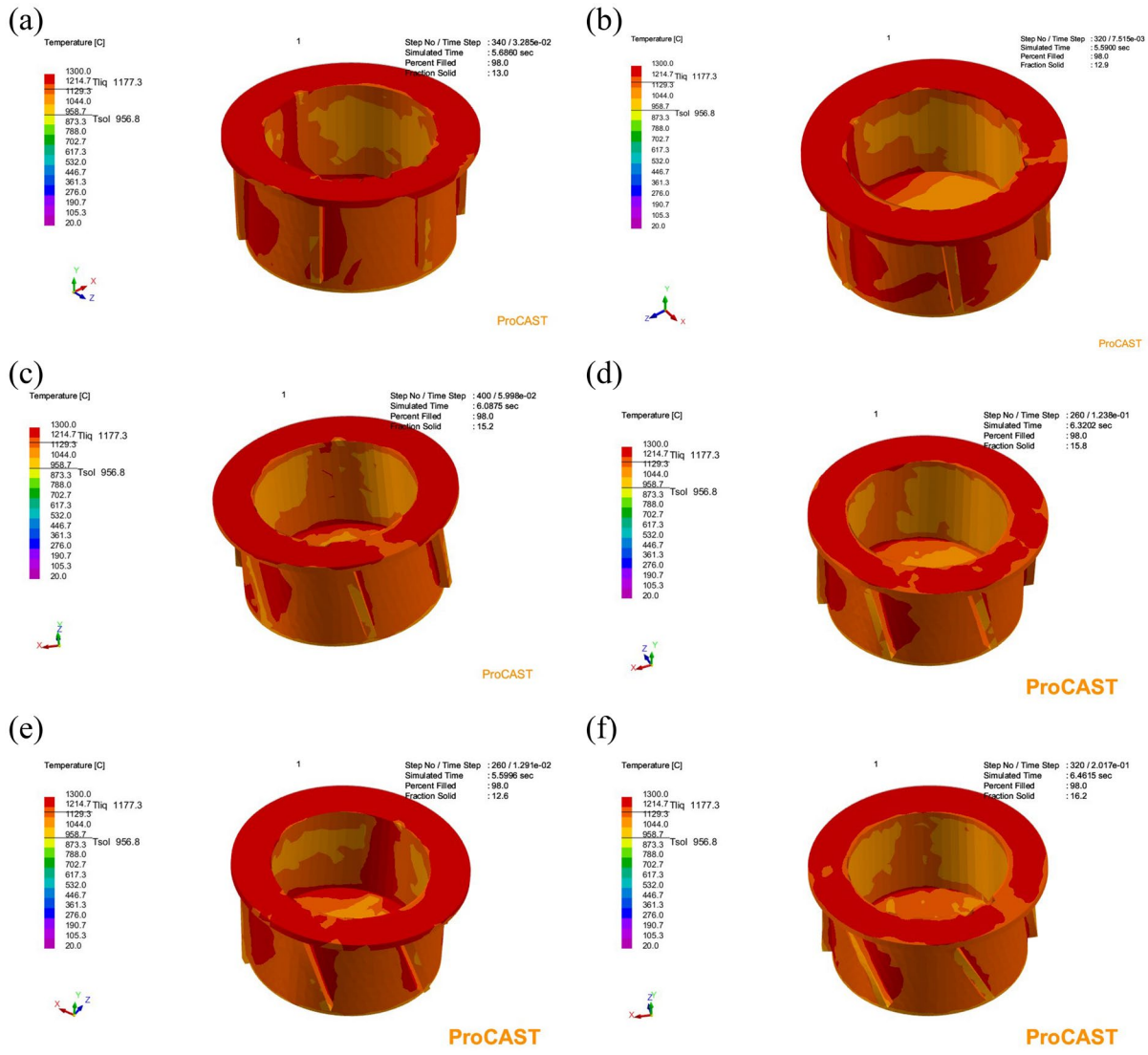

Fig. 4. Temperature distribution states of different mold schemes: (a) 0°, (b) 5°, (c) 10°, (d) 15°, (e) 20°, (f) 25°

As illustrated in Fig.4(a) through Fig.4(f), an increase in angle results in a more uniform temperature distribution within the casting. It is noteworthy that the circumferential groove solidifies at a faster rate than other regions. Similarly, the temperature differential indicates that the process of solidification commences from the sides. However, in contrast to other angles, the temperature distribution in Fig.4(c), Fig.4(d), and Fig.4(f) is notably superior, which is advantageous for the mitigation of defects that might arise during the subsequent solidification phase. Moreover, the comprehensive temperature gradient of the casting demonstrates that molds with smaller angles to a certain extent alleviate the feeding issue during the casting's cooling process, thus preventing complications such as insufficient pouring due to metal shrinkage during cooling [11, 12]. It can be reasonably deduced that the utilization of molds with moderate angles will ensure adequate feeding during the pouring and cooling phases. This configuration allows the metal liquid within the pouring system to effectively counteract the shrinkage of the metal liquid in the circumferential groove, due to the influence of gravity. This prevents any under-pouring issues. Furthermore, it ensures that the temperature gradient is aligned with the pouring direction, thereby facilitating sequential solidification and resulting in a casting with a dense and robust internal structure.

In light of the aforementioned findings, both the 10-degree and 15-degree mold configurations exhibit no discernible zones of elevated overall temperatures within their respective flow and temperature fields. Notwithstanding the extended filling durations, both setups yield more uniform temperature distributions and liquid phase areas. The majority of the molten metal is located in the transition zone, spanning temperatures from 956.8°C to 1177.3°C, where a liquid-to-solid transformation occurs, featuring coexisting liquid and solid phases. This dual-phase condition results in a more gradual temperature transition compared to single-phase scenarios, as previously documented in reference [13]. In cast iron containing

phosphorus, the circumferential groove angles of the casting mold exhibit notable variation, exerting a substantial influence on the inflow rate and stability. This, in turn, gives rise to a pronounced temperature gradient between the molten metal in the transition zone and the single-phase zone. This gradient frequently results in the formation of hot spots in regions that cool at a slower rate, a phenomenon that is deleterious to the proper feeding of shrinkage cavities during the cooling process. Therefore, in consideration of the flow dynamics and feeding capabilities during the cooling process, the implementation of mold configurations with angles of 10 and 15 degrees is more conducive to the production of high-quality cast iron castings with phosphorus, thereby enhancing the efficiency of electrolytic aluminum production.

3.3. Effect of Varying Groove Angles on the Solidification Process

The influence of varying groove angles on the solidification process of components is evident and distinctive. By examining the solid fraction, cooling rate, and the distribution of shrinkage cavities and porosity across different gating systems, it is possible to elucidate the solidification behaviors of phosphorus cast iron castings under differing groove angles.

3.3.1. Solid fraction

The solid fraction of castings derived from molds featuring varying groove angles is depicted in Fig.5. As evidenced by the simulation outcomes, the presence of grooves resulted in the partial solidification of the castings upon the completion of the filling process within the phosphorus cast iron wall.

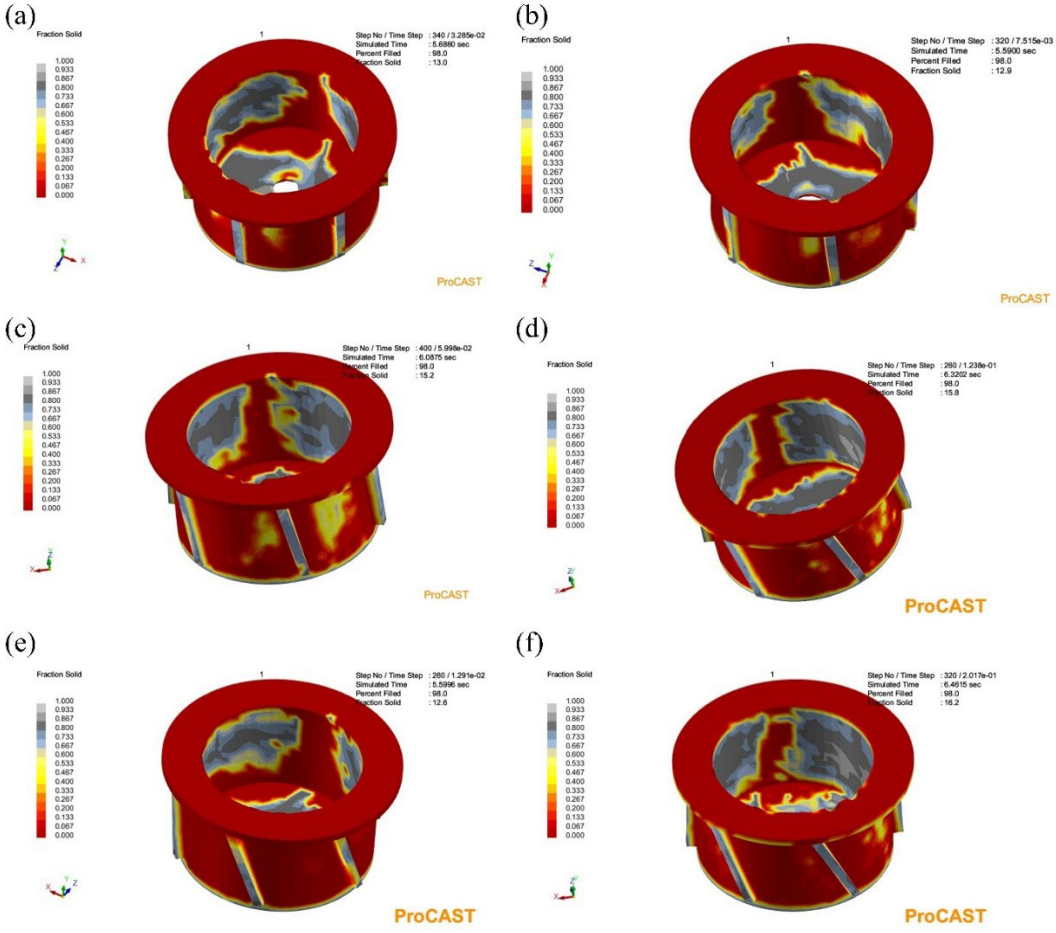

Fig.5 Solid fraction of different mold schemes:(a) 0°, (b) 5°, (c) 10°, (d) 15°, (e) 20°, (f) 25°

As shown in Fig.5(a) to Fig.5(d), it can be observed that with the increase of the circumferential groove angle, the solidification area of the casting gradually increases, and the solidification sequence becomes more orderly. However, as the angle continues to increase, the solidification area begins to shrink. In the mold with a 25-degree angle, the solidification sequence is relatively chaotic, and the layered changes in sequential solidification are not as pronounced as in the previous four mold designs. Nevertheless, in all the schemes, there is a situation where three sides are pressing against each other. In this region, a local slowdown in the solidification rate may occur, leading to the formation of isolated liquid zones. This can cut off the feeding channels, resulting in defects in this area. Narrowing the feeding channels for the cooling and shrinkage process of the casting will not ensure the

compactness of the casting [14], ultimately leading to poor quality of the phosphorus cast iron. During the sequential solidification process of the casting, the inlet will solidify after the mold cavity has completed solidification.

The comparative analysis of the solid fraction reveals that, regardless of the mold scheme utilized, the solidification sequence of the casting progresses from the interior to the exterior, ensuring a sequential solidification process. Nevertheless, the temporal rate of change in the solid fraction during solidification has a significant impact on the overall thermal equilibrium and the evolving trend of thermal gradients within the temperature field. The temperature field, in turn, governs the feed length between dendritic arms of the metal [15], thereby influencing the microstructural density of the casting. At the onset of casting solidification, the solid fraction values across the casting surface are predominantly uniform, with no isolated liquid regions discernible. This analysis unequivocally reveals that the mold scheme oriented at 15 degrees excels in solid fraction performance, yielding a notably more uniform solidification effect.

3.3.2. Shrinkage porosity distribution

The shrinkage porosity and shrinkage cavities observed in castings produced under various mold schemes are illustrated in Fig.6. As shown in Fig.6(a) to Fig.6(f), these defects are primarily concentrated in the upper annular and bottom regions of the castings. With the angle increment, the distribution of shrinkage porosity and cavities in the bottom region becomes increasingly focused. In the upper annular region, with the exception of the 20-degree angle, the defects are uniformly spread across the top of the circumferential groove, showing minimal variation. Furthermore, shrinkage porosity and shrinkage cavity defects are also detected in the isolated liquid phase regions, as identified by the solid fraction analysis of the castings.

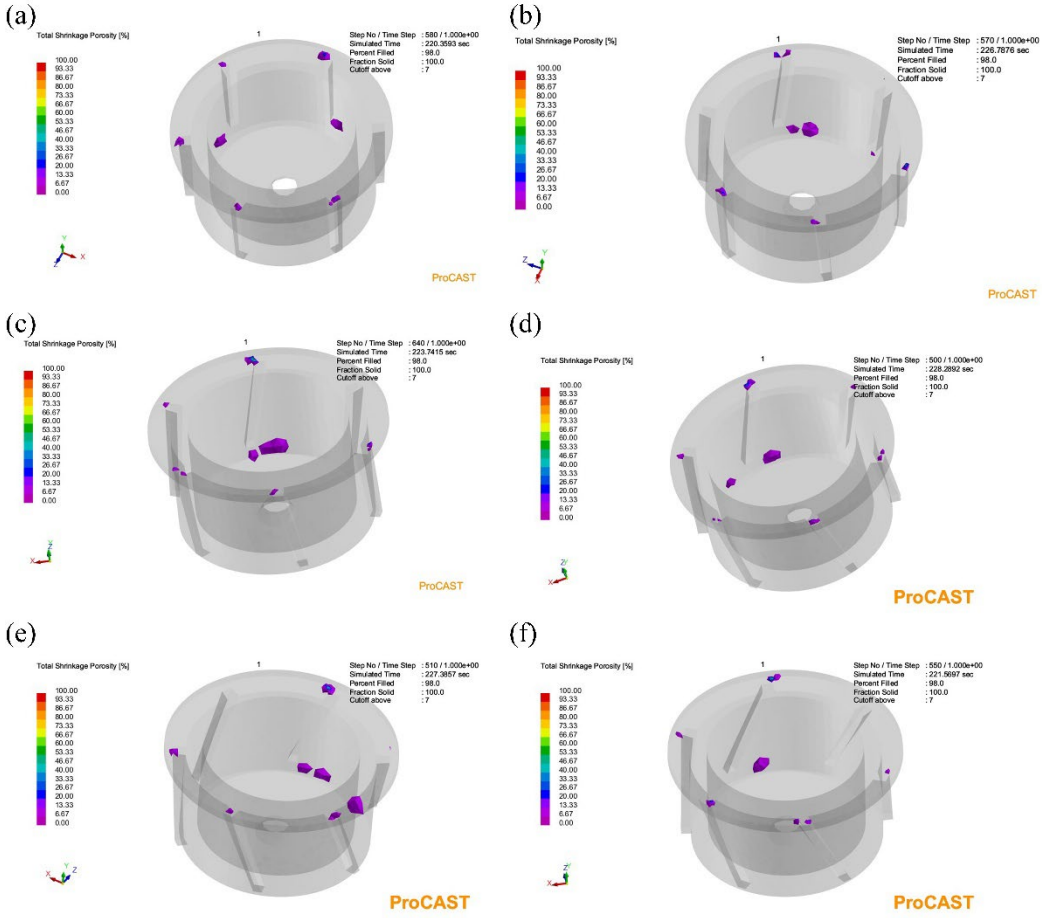

Fig.6 Distribution of shrinkage cavities and porosity in different mold designs:(a) 0°(b) 5° (c) 10°(d) 15° (e) 20° (f) 25°

Subsequently, the software was employed to analyze shrinkage porosity across various mold configurations, and the findings are detailed in Table 4. By the extraction and calculation of shrinkage porosity volumes through the use of numerical simulation software, the volume of shrinkage porosity within the casting was determined. As demonstrated by the data presented in the table, the 25-degree mold scheme exhibits the lowest shrinkage volume, with a value of approximately 0.67cm³.

Table 4.
Volume of shrinkage cavities and porosity in different casting molds

Casting mold	0°	5°	10°	15°	20°	25°
Shrinkage volume	0.92cm^3	0.71cm^3	1.07cm^3	0.90cm^3	1.24cm^3	0.67cm^3

3.4. Comparison and Analysis of Results Across Six Casting Mold Schemes

By analyzing the performance of six different gating schemes during the filling process and solidification process, the flow field state, temperature field state, solids ratio and the distribution of shrinkage porosity of each scheme were scored on a scale of 1-3 points (higher scores indicate better performance). Subsequently, the overall score is used to evaluate and determine the advantages and disadvantages of each pouring mold scheme. For details about the scoring results and scheme comparisons in the Table 5.

Table 5.
Comparison of mold schemes from different angles

Casting mold angle scheme	Flow field state	Temperature field state	Solid fraction	Shrinkage porosity distribution	Overall score
0°	2	1	2	2	7
75°	1	1	2	3	7
10°	3	3	2	1	9
15°	3	3	3	2	11
20°	3	1	1	1	6
25°	2	2	1	3	8

A comprehensive comparative analysis of the casting projects presented in Table 5 reveals that the mold design with a circumferential groove angle of 15 degrees is the optimal choice, followed by the mold design with a circumferential groove angle of 10 degrees, and the mold design with a circumferential groove angle of 20 degrees is the least favorable. The findings suggest that the circumferential groove angle present in the casting structure may influence the quality of the resulting phosphorous cast iron castings. The software simulation indicates that the casting scheme for the mold with a circumferential groove angle of 15 degrees can ensure superior quality of the castings obtained. During the pouring process, the mold cavity fills smoothly, and the temperature field distribution is optimal, which is conducive to the formation of a dense microstructure. The process of sequential solidification is effectively regulated, thereby facilitating the production of castings that exhibit optimal performance. The volume of shrinkage porosity defects is diminished, thereby facilitating the production of high-quality castings.

4. Casting Test Analysis and Discussion

By means of simulation and calculation, the angular dimensions of the circumferential groove in phosphorus cast iron have been determined. The results demonstrate that a mold pouring configuration featuring a groove angle of 15 degrees represents the optimal approach. To substantiate the viability of this configuration, it is imperative to engineer a carbon block mold and employ the CAFE module to simulate the casting organization orientation within the phosphorus cast iron casting. Concurrently, it is essential to obtain actual casting specimens for microstructural validation through electron backscatter diffraction (EBSD) analysis[16-18].

4.1. CAFE simulation

4.1.1. Parameter settings

According to the requirements of the materials used in the parts, after the *Dt* =10 (*Dt* means Delta time) and Gibbs-Thompson Coefficient is 2e-07 were set, the system can auto calculate parameter of the interfacial mobility (m), solute partition coefficient (k) and solute diffusion coefficient(*D1*). Also, each element is calculated using the software to obtain the standard value of the nucleation model parameter nucleation supercooling (*a2*) and the average value of nucleation supercooling (*a3*). Moreover, it is necessary to select the area for calculation, as illustrated in Fig.7. The entirety of the shape nucleation calculation is performed in accordance with the tenets of Gaussian nucleation theory [19].

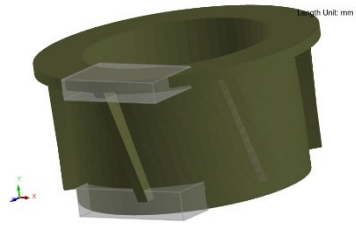

Fig. 7. Selection of the module calculation area

4.1.2. Undercooling and casting stress

The cooling process, along with the associated undercooling behavior and casting stress of phosphorus cast iron parts, is vividly depicted in Fig.8, which showcases the outcomes of simulation calculations.

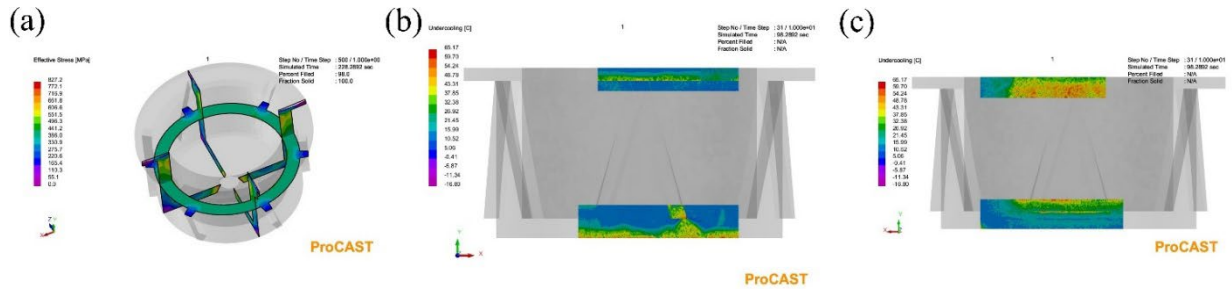

Fig. 8. Casting stress and undercooling:(a) Casting stress, (b) Outer undercooling, (c) Inner undercooling

Fig.8(a) illustrates the distribution of casting stress in phosphorus cast iron across the XY, YZ, and XZ planes. It is noteworthy that the internal casting stress along the same horizontal line on all three planes exceeds the external casting stress. This indicates that the carbon block experiences relatively lower stress during the casting molding process, thereby extending its operational lifespan in the aluminum electrolysis process to a certain extent. Fig.8(b) illustrates that the external undercooling is significantly less than the internal undercooling observed in Fig.8(c). This discrepancy suggests that superior and more complete contact with the mold was achieved during the cooling and solidification of the phosphorus cast iron melt. Consequently, the casting surface in this region is smoother. This enhanced contact accelerates the cooling rate of the metal melt [20], resulting in a broader secondary dendrite arm spacing [21]. The resulting microstructure is more compact, which leads to improvements in tensile strength, hardness, and elongation properties.

4.1.3. Grain orientation difference distribution

The grain orientation difference distribution map for the phosphorous cast iron component, derived from simulation computations, is depicted in Fig.9.

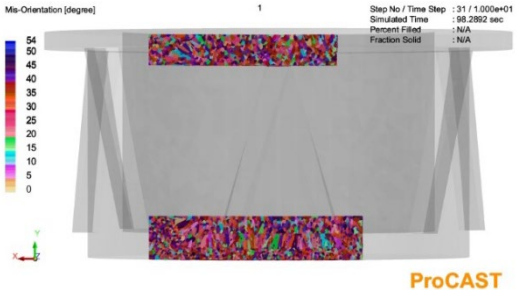

Fig. 9. Distribution of grain orientation differences

As illustrated in the Fig.9, the upper region demonstrates the exclusive development of columnar crystals, while the central equiaxed zone, accompanied by a smaller surface fine grain zone, exhibits a distinct set of characteristics. In contrast, the lower region exhibits a distinct distribution of microstructural zones, including a surface fine grain zone, a columnar crystal zone, and a central equiaxed zone. A notable accumulation of columnar crystals is evident in the vicinity of the steel claw, which may potentially lead to cracking during operational use, as previously observed [22]. Therefore, a comprehensive examination and practical experimentation are essential to elucidate the underlying microstructural characteristics.

4.2. Casting test results and analysis

Fig.10 depicts the sampling sites of the molded castings derived from a mold pouring process featuring a 15-degree circumferential groove angle, along with the designated test surfaces for EBSD analysis. The resulting castings demonstrate that the surface quality of the phosphorus cast iron castings is of an exemplary standard. The circumferential grooves are formed with precision, and the castings are filled to a high degree of accuracy. It is noteworthy that no significant defects, such as inadequate pouring or macroscopic cracks, were identified on the castings' surfaces.

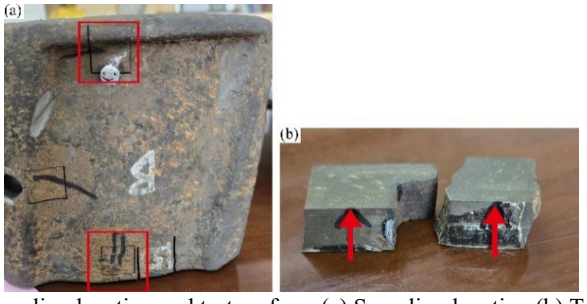

Fig. 10. Sampling location and test surface: (a) Sampling location (b) Test surface

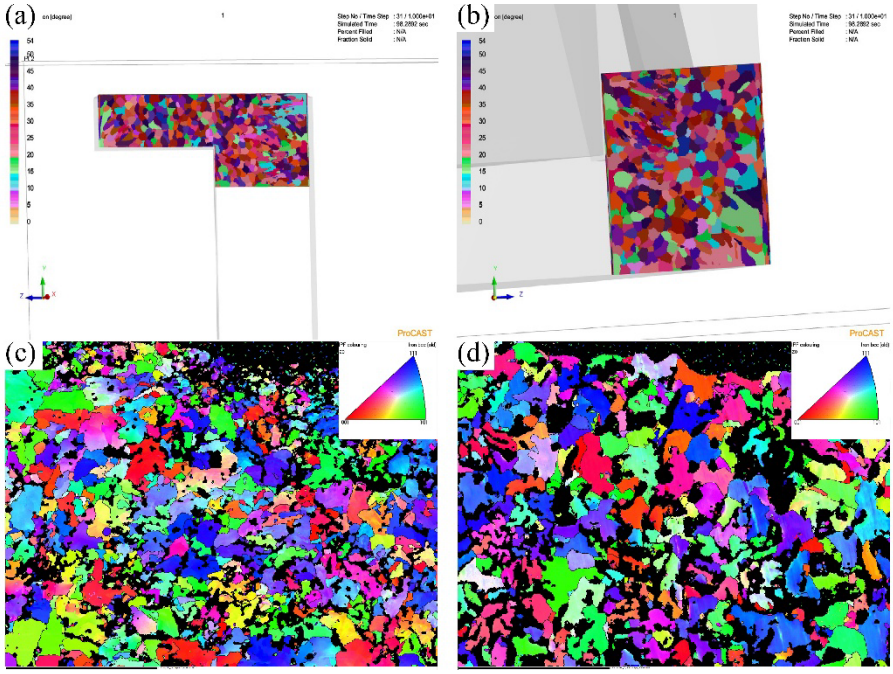

Fig. 11. Grain orientation distribution map: (a) Orientation distribution of upper grain, (b) Orientation distribution of lower grain, (c) Grain Orientation Distribution (Close to Steel), (d) Grain Orientation Distribution (Close to Carbon)

Fig.11 presents the grain orientation distribution maps derived from both the simulation and the actual testing conducted on the test surface of the casting. As illustrated in Fig.11(a) and Fig.11(b), the disparity in grain orientation near the carbon block is slightly greater than that near the steel claw, yet the grain distribution remains relatively uniform. Fig.11(c) and Fig.11(d) demonstrate a markedly diminished number of actual grain orientations, as indicated by IPF-Z0. Moreover, the orientation distribution map in the vicinity of the steel exhibits a more refined and concentrated arrangement of grains. The diverse orientations of these grains interlace in intricate patterns, impeding crack propagation [23]. In contrast, the grain distribution in the vicinity of the carbon is more dispersed, which facilitates crack propagation in this region. This property fulfills the requisite brittleness for phosphorus-containing iron in the electrolytic aluminum industry.

5. Conclusions

Phosphorus cast iron casting process under different groove angles was calculated by simulation software, and the cast iron organizations at different positions of the interface were analyzed. The following conclusions were get:

1. The filling and solidification process of phosphorus cast iron at different angles are quite different: the filling speed, temperature distribution and the solid phase ratio at 15 degree angles are relatively uniform, which is conducive to the formation of phosphorus cast iron. Also, under this angle, sequential solidification can be basically realized, which can lead to obtain the low porosity casting.
2. The micromorphology calculated by CAFE is close to the actual test results, and the micrograins near the carbon block are relatively sparse. This can not only ensure the connection performance of phosphorus cast iron, but also make the connection have a certain brittleness. It is easy to recycle the steel claw in electrolytic aluminum anode assembly.

Acknowledgments

The authors thank Guizhou Lines Machine Design and Manufacture Co., Ltd. for helping and enabling the use of company resources to perform experiments.

References

[1] Hop, J., Store, A., Foosnaes, T. & Oye, H.A. (2005). Chemical and physical changes of cathode carbon by aluminium electrolysis. *Mineral Processing and Extractive Metallurgy*. 114(3), 181-187. https://doi.org/10.1179/037195505X63376.

[2] Senanu, S., Wang, Z., Ratvik, A.P. & Grande, T. (2020). Carbon cathode wear in aluminium electrolysis cells. *The Journal of The Minerals, Metals & Materials Society*. 72(1), 210-217. https://doi.org/10.1007/s11837-019-03717-z.

[3] Allard, F., Soucy, G., Rivoaland, L. & Désilets, M. (2015). Thermodynamic and thermochemical investigation of the deposits formed on the cathode surface of aluminum electrolysis cells. *Journal of Thermal Analysis and Calorimetry*. 119, 1303-1314. https://doi.org/10.1007/s10973-014-4288-z.

[4] Li, Q., Liang, J., Liu, B., Peng, Z. & Wang, Q. (2014). Effects

of cathodic voltages on structure and wear resistance of plasma electrolytic oxidation coatings formed on aluminium alloy. *Applied Surface Science*. 297, 176-181. https://doi.org/10.1016/j.apsusc.2014.01.120.

[5] Li, T.F., Tao, W.J., Wang, Z.W. & Liu, X.Z. (2020). Effects of the size of cast iron and stub on the physical field of anode in aluminium reduction cell. *Journal of Northeastern University.* 41(6), 828-834. https://doi.org/10.12068/j.issn.1005-3026.2020.06.012.

[6] Zhang, Y.H. & Ding, H.M. (2016). Optimization of cast iron casting process for the cathode carbon block. *Light Metals*. 4, 31-34,43. https://link.oversea.cnki.net/doi/10.13662/j.cnki.qjs.2016.04.008.

[7] Huang, Y.B., & Yuan, Z.H. (1998). Study on the composition of phosphorus iron for aluminum electrolysis. *Light Metals*, 2, 37-39. https://link.oversea.cnki.net/doi/10.13662/j.cnki.qjs.1998.02.008.

[8] Dojka, R., Jezierski, J. & Campbell, J. (2018). Optimized gating system for steel castings. *Journal of Materials Engineering and Performance*. 27, 5152-5163. https://doi.org/10.1007/s11665-018-3497-1.

[9] Dojka, R., Jezierski, J. & Tiedje, N.S. (2019). Geometric Form of Gating System Elements and Its Influence on the Initial Filling Phase. *Journal of Materials Engineering and Performance*. 28, 3922-3928. https://doi.org/10.1007/s11665-019-03973-9.

[10] Dhisale, M., Vasavada, J. & Tewari, A. (2022). An approach to optimize cooling channel parameters of low pressure die casting process for reducing shrinkage porosity in aluminium alloy wheels. *Materials Today: Proceedings*. 62(6), 3189-3196. https://doi.org/10.1016/j.matpr.2022.03.478.

[11] Zhang, F., Kang, Y.L., Yang, L.Q. & Ding, R.H. (2010). Effects of pouring temperature on the cooling rules of alloy melts and the semi-solid microstructure. *Chinese Journal of Engineering*. 32(11), 1453-1458. https://doi.org/10.13374/j.issn1001-053x.2010.11.014.

[12] Qin, T. & Xu, N.B. (2012). Research on influence of pouring temperature on quality of rotor casting by using software ProCAST. *Modern Cast Iron*. 32(03), 74-77. https://doi.org/10.3969/j.issn.1003-8345.2012.03.014.

[13] Zheng, Q., Xiao, Y., Zhang, T., Zhu, P., Ma, W. & Liu, J. (2020). Numerical simulation of latent heat of solidification for low pressure casting of aluminum alloy wheels. *Metals*. 10(8), 1024, 1-12. https://doi.org/10.3390/met10081024.

[14] Vijayaram, T.R., Sulaiman, S., Hamouda, A.M.S. & Ahmad, M.H.M. (2006). Numerical simulation of casting solidification in permanent metallic molds. *Journal of materials processing technology*. 178(1-3), 29-33. https://doi.org/10.1016/j.jmatprotec.2005.09.025.

[15] Thompson, S., Cockcroft, S.L. & Wells, M.A. (2004). Advanced light metals casting development: solidification of aluminium alloy A356. *Materials science and technology*. 20(2), 194-200. https://doi.org/10.1179/026708304225011199.

[16] Liu, F., Ma, X.T., Liu Z.W. & Xie, H.M. (2023). Electron backscatter diffraction technology and its application in the study of micro-mechanical behavior. *Mechanics and Practice*. 45(6), 1321-1330. https://doi.org/10.6052/1000-0879-23-301.

[17] Radovic, Z. & Lalovic, M. (2005). Numerical simulation of steel ingot solidification process. *Journal of Materials Processing Technology*. 160(2), 156-159. https://doi.org/10.1016/j.jmatprotec.2004.07.094.

[18] Zhao, S. & Wang, S.J. (2025). Research progress in crystal plasticity deformation mechanisms and their numerical simulation methods. *Manufacturing Technology & Machine Tool*. 1-13. https://doi.org/10.19287/j.mtmt.1005-2402.2025.02.013.

[19] Wang, J.L., Lai, C.B., Wang F.M., Zhang J.M. & Ren, W. (2009). Mechanism and application of the CAFE model. *Journal of Iron and Steel Research.* 21(10), 4. https://doi.org/10.13228/j.boyuan.issn1001-0963.2009.10.004.

[20] Cramb, A.W. (2005). Solidification and steel casting. *Fundamentals of Metallurgy.* 399-452. https://doi.org/10.1533/9781845690946.2.399.

[21] Shen, Y., He, G.Q., Tian, D.D., Fan, K.L., Liu, X.S. & Mo, D.F. (2014). Effect of secondary dendrite arm spacing on tensile property and fatigue behavior ofa319 aluminum alloy. *Journal of Materials Research.* 28(8), 587-593. https://doi.org/10.11901/1005.3093.2014.117.

[22] Brust, A.F., Niezgoda, S.R., Yardley, V.A. & Payton, E.J. (2019). Analysis of misorientation relationships between austenite parents and twins. *Metallurgical and Materials Transactions A*. 50, 837-855. https://doi.org/10.1007/s11661-018-4977-5.

[23] Pan, C.C., Ma, C. & Xia, D.H. (2020). Estimation for Relevance of Atmospheric Corrosion Initiation with Surface Texture of Several Metallic Materials by Electron Backscattering Diffraction. *Journal of Chinese Society for Corrosion and protection*. 39(6), 495-503. https://doi.org/10.11902/1005.4537.2019.232.